Organic Electronics 15 (2014) 893–903

Contents lists available at ScienceDirect

Organic Electronics

journal homepage: www.elsevier.com/locate/orgel

Letter

High-efficiency polymer solar cells by blade coating in chlorine-free solvents

Pei-Ting Tsai [a], Chia-Ying Tsai [b], Chun-Ming Wang [a], Yu-Fan Chang [c], Hsin-Fei Meng [a,*], Zhi-Kuan Chen [d,*], Hao-Wu Lin [e,*], Hsiao-Wen Zan [c], Sheng-Fu Horng [f], Yi-Chun Lai [c], Peichen Yu [c]

[a] Institute of Physics, National Chiao Tung University, Hsinchu 300, Taiwan
[b] Institute of Photonics Technologies, National Tsing Hua University, Hsinchu 300, Taiwan
[c] Department of Photonics and the Institute of Electro-Optical Engineering, National Chiao Tung University, Hsinchu 300, Taiwan
[d] Institute of Advanced Materials, Nanjing University of Technology, Nanjing 210009, China
[e] Department of Materials Science and Engineering, National Tsing Hua University, Hsinchu 300, Taiwan
[f] Department of Electrical Engineering, National Tsing Hua University, Hsinchu 300, Taiwan

ARTICLE INFO

Article history:
Received 26 August 2013
Received in revised form 27 December 2013
Accepted 21 January 2014
Available online 4 February 2014

Keywords:
PBDTTT-C-T
Chlorine-free solvents
Blade coating
Polymer solar cells

ABSTRACT

High-performance polymer cells are typically fabricated by employing toxic solvents such as dichlorobenzene and chlorobenzene. In this study, blade coating with the chlorine-free solvents toluene and xylene is applied to polymer solar cells that contained the low band-gap polymer PBDTTT-C-T blended with [6,6]-phenyl-C71-butyric acid methyl ester ([70]PCBM). The highest efficiencies of the cells fabricated in toluene and xylene solutions were 6.09% and 6.11%, respectively. Atomic force microscopy images show that the films formed by blade coating using toluene and xylene were extremely smooth, with roughness of only 1 nm. This blade coating has a rapid-drying in a few seconds without the long-running thermal or solvent annealing. The possibility of high-volume environmentally-friendly fabrication of efficient polymer solar cells with minimal material waste is thus demonstrated using a combination of chlorine-free solvents and blade coating.

1. Introduction

Polymer solar cells based on a blend of conjugated polymers as electron donors and fullerene derivatives that serve as electron acceptors have exhibited a ever-increasing power conversion efficiency over the past decade. Recently efficiency over 8% is reported for low band-gap polymers [1–9]. However, most high-efficiency polymer solar cells have been fabricated by spin coating using chlorine-containing solvents such as dichlorobenzene, because of their high boiling point and slow evaporation. The desired donor–acceptor phase separation in the tens of nanometer scale is usually achieved by using a slow solvent evaporation method, i.e. solvent annealing, after spin coating in dichlorobenzene solvent [10]. In addition, material solubility and molecular compatibility are important considerations in designing polymer composites. The solubility of the donor polymers have a profound effect on the film morphology and solar cell performance [11–18]. Most low band-gap polymers exhibit poor solubility in commonly used chlorine-free solvents such as toluene and xylene. Therefore, uniform film with proper thickness is difficult to fabricate using chlorine-free solvents, and the solar cells by them usually exhibit unsatisfactory efficiencies [19,20]. However, solvents containing chlorine are

* Corresponding authors. Tel.: +886 3 5731955 (H.-F. Meng), tel.: +86 25 83587982 (Z.-K Chen), tel.: +886 3 5715131x33879 (H.-W. Lin).
E-mail addresses: meng@mail.nctu.edu.tw (H.-F. Meng), iamzkchen@njut.edu.cn (Z.-K. Chen), hwlin@mx.nthu.edu.tw (H.-W. Lin).

http://dx.doi.org/10.1016/j.orgel.2014.01.018
1566-1199/

highly toxic and environmentally hazardous. This dilemma is a major obstacle to the potential mass production of polymer cells despite of the advantage of low-cost large-area solution fabrication. Recently, a 6.1% power conversion efficiency has been reported for polymer solar cells spin coated in a halogen-free solvent [21]. However, using spin coating alone is incompatible with high-volume production because it produces large amounts of material waste and is incompatible with the roll-to-roll process. Therefore, developing a chlorine-free polymer solar cell process involving small amounts of material waste and the compatibility to roll-to-roll fabrication is crucial.

This study focuses on the low band-gap polymer PBDTTT-C-T, [22] which exhibit an unusually high solubility in the chlorine-free non-toxic solvents toluene and xylene. Blade coating, rather than conventional spin coating, is used to deposit the active layer [23–26]. Blade coating has the advantage of exhibiting large-area uniformity, small amount of material waste, preventing of inter layer dissolution, and being compatible with the roll-to-roll process. Blade coating involves a rapid drying process that prevents the fabrication throughput from being slowed by the conventional solvent annealing process. A high efficiency of 6.1% was achieves by blade coating for solar cells comprising a combination of PBDTTT-C-T and [70]PCBM that were dissolves in toluene and xylene. In addition, the performance of these devices was insensitive to the solvent regardless of whether chlorine was included. By contrast, the archetypical polymer poly(3-hexylthiophene) (P3HT) and another low band-gap polymer poly{(benzo-2,1,3-thiadiazol-4,7-diyl)-alt-(3′,4″di(2-octyldodecyl)-2,2′;5′,2″;5″,2‴-quaterthiophen-5,5‴-diyl)}(POD2T-DTBT) were much less soluble in chlorine-free solvent than in dichlorobenzene. In sharp contrast to PBDTTT-C-T these solar cells exhibit much lower efficiency using the former solvents. The capability of using donor polymers exhibiting high solubility in chlorine-free solvents to achieve high-throughput and environmental friendly production of efficient polymer cells is demonstrated.

2. Experimental

Fig. 1 shows the energy band diagrams, detailing the work functions of the organic solar cells and the chemical structures of the active layer materials used in this study. The energy level of the lowest unoccupied molecular orbital (LUMO) and highest occupied molecular orbital (HOMO) relative to the vacuum are labeled [17,22]. PBDTTT-C-T was purchased from Solarmer materials Inc. The PBDTTT-C-T and POD2T-DTBT exhibited low band-gaps of 1.58 eV and 1.59 eV, respectively, whereas P3HT exhibited a band-gap of 1.9 eV [23]. Fig. 2a illustrates the blade coating method and Fig. 2b is the picture of the auto-blade machine. The blade coater is cylindrically shaped and the gap between the cylinder and the substrate was 120 μm. The solution was delivered to the gap by using a pipette and the motion of the blade formed a wet film. The blade speed ranged from 20 to 400 mm/s. The blade coating procedure was executed on a hot plate. After coating the wet film, the hot air was applied to evaporate the remaining solvent in approximately 1–10 s. The thickness of the remaining dry film could be controlled by adjusting the blade speed. The blade coating was performed in a self-fabricated machine, which was controlled using a linear motor.

Polymer solar cells were fabricated on pre-patterned indium-tin-oxide (ITO) glass with the device structure of ITO/PEDOT:PSS (poly-(3,4-ethylenedioxythiophene):poly-(styrenesulfonate) (CLEVIOS™ PVP AI4083, purchased from HC Starck)/PBDTTT-C-T:[70]PCBM/Ca/Al [70]PCBM was purchased from Solenne. The ITO-coated glass substrates were treated in an ultrasonic bath for 60 min in acetone, subsequently rinsed three times with deionized water and cleaned using UV ozone cleaner for 30 min. The 40 nm PEDOT:PSS layer was spin coated at 2200 rpm on the ITO substrate and baked at 200 °C in air for 15 min. To prepare the PBDTTT-C-T and [70]PCBM solutions, PBDTTT-C-T and [70]PCBM powders were mixed. The weight ratio of the PBDTTT-C-T to [70]PCBM was fixed at 1:1.5. The mixed powder was dissolved using various solvents such as toluene, chlorobenzene, and xylene.

To perform blade coating, approximately 3% (1,8-diiodooctane (DIO)/solvents (toluene, chlorobenzene, and xylene), v/v) DIO was used as an additive and was included to improve photovoltaic results. The mixed solution was heated on a hot plate at 80 °C. The active layers were coated using an auto-blade machine, as shown in Fig. 2. Rapid-drying blade coating was performed using a hot plate at 80–90 °C. The solution (70 μL) was coated using the auto-blade machine at approximately 260 mm/s to cover the 4-mm^2 active area of the device with wet film. The thickness of the active layer was 100–120 nm. Hot air produced by a hair dryer containing a diffuser was applied to enhance the drying and uniformity. Dry films formed in approximately 3 s for toluene and chlorobenzene, and 10 s for xylene. The air temperature was approximately 70 °C. To perform spin coating, approximately 3% DIO was a added to the main solvents. The mixed solution was then heated on a hot plate at 80 °C. The thickness of the active layer was 100–120 nm when spin coated at a spin rate of 1000 rpm for 40 s. The wet film was subsequently dried slowly for 2 h during the solvent annealing process. Finally, a Ca(35 nm)/Al(100 nm) electrode was formed on the top of the active layer by using thermal evaporation in a vacuum chamber with a base pressure below 3.0×10^{-6} Torr. Regarding the POD2T-DTBT devices, only Al was evaporated without Ca film. All of the devices were packaged in a glove box and measured in an ambient environment.

To determine the characteristics of the solar cell devices, the power conversion efficiency (PCE) was measured using a solar simulator (XES-301S, SAN-EI) under AM1.5G of irradiation. The incident photon conversion efficiency (IPCE) is defined as the average number of carriers per incident photon. To measure the IPCE, a 300-W Xenon lamp (Newport 66984) and a monochromator (Newprot 74112) were used as light sources. The beam spot on the sample was a square, and the spot size was 3 mm^2. A calibrated silicon photodetector with a known spectral response (Newport 818-UV). The IPCE was measure using a lock-in amplifier (Standard Research System, SR830), an optical chopper unit (SR540) operating at a 260-Hz chopping frequency, and a 1 Ω resistor in a shunt connection to convert the photocurrent to voltage. There is a sharp

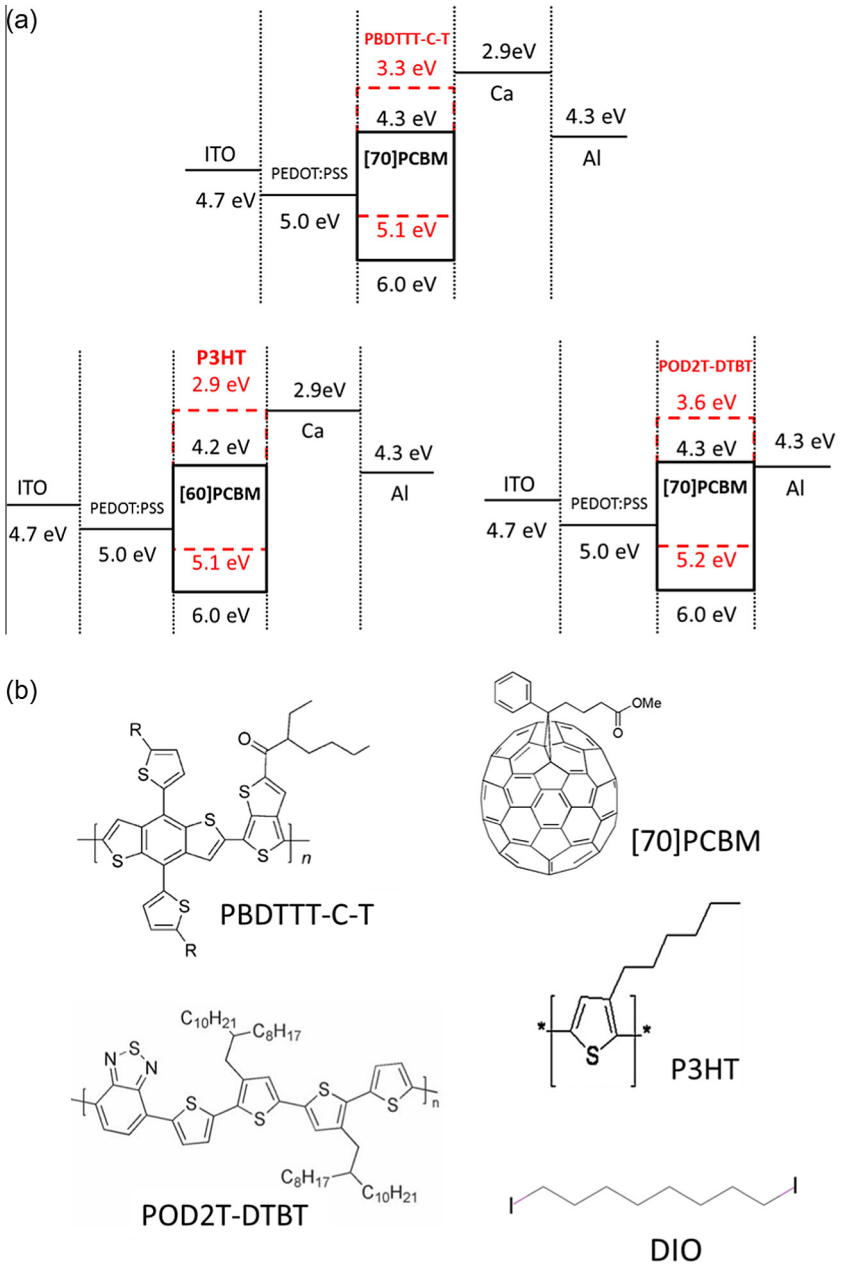

Fig. 1. (a) Energy band diagrams and (b) the chemical structures in this work.

peak around 825 nm in our solar simulator as shown in Fig. 3. Aside from this peak the simulator power spectrum was quite similiar to the AM1.5 reference solar spectrum. The 825 nm peak contributed to some extra photo-current when the absorption material has low band gap as in our case. The IPCE shown below extends in the long wavelength region beyond 825 nm. The extra photo-current due to the 825 nm peak could be estimated by integrating the product of this peak and the IPCE spectrum. In all the data below the short-circuit current is deducted by this extra current and the power conversion efficiency is adjusted correspondingly. To analyze the films fabricated using various deposition methods, the surface morphology and phase were monitored using an atomic force microscope (AFM, Dimension 3100, Digital Instruments). The high-resolution morphology was monitored using a variable temperature scanning probe microscope (VT SPM, SPA-300HV). The absorption spectrum was measured using a UV–visible spectrophotometer (HP8453).

3. Results and discussions

3.1. Spin coating

Before presenting the results of using blade coating, the data regarding the solar cells fabricated using conventional

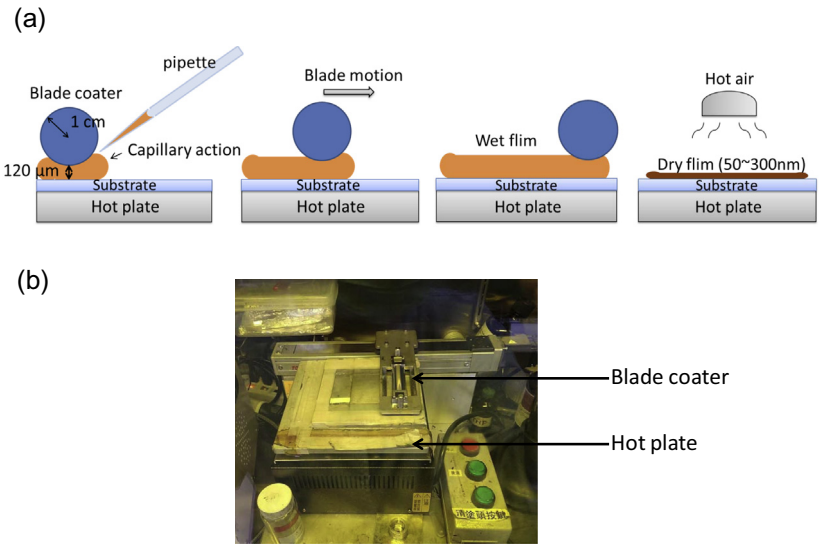

Fig. 2. (a) The blade coating method and (b) the auto-blade machine.

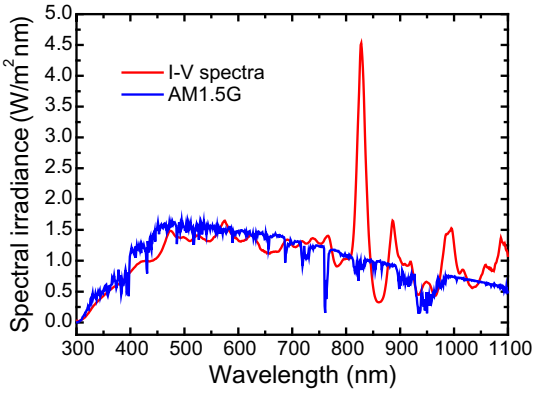

Fig. 3. AM1.5 reference solar spectrum and solar simulator spectrum.

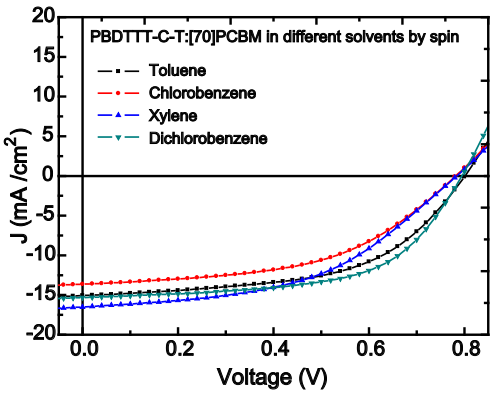

Fig. 4. *J–V* curves of PBDTTT-C-T/[70]PCBM solar cells with active layers dissolved in different solvents using spin coating method.

spin coating are presented. The current density–voltage (*J–V*) characteristics and photovoltaic parameters exhibited by the four solvents, dichlorobenzene, chlorobenzene, toluene, and xylene, when using a solar simulator are shown in Fig. 4 and Table 1. Dichlorobenzene and chlorobenzene contain chlorine, and toluene and xylene do not. The boiling points of these solvents are 180 °C, 131 °C, 138 °C and 111 °C respectively. The dichlorobenzene device exhibited the highest power conversion efficiency, which was 6.42%. This value is only slightly lower than the value produces in a previous study (7.59%) in which the same process was used. Because it exhibited a high boiling point and underwent a slow evaporation process, the blend film composed of dichlorobenzene became dry after approximately 2 h of solvent annealing, in which the polymer donor and the fullerene acceptor performed the phase separation. The other three solvents produced lower efficiency, most likely because the evaporation of dichlorobenzene occurred more quickly than did that of the other solvents. Nevertheless, the efficiency was over 6% when toluene and xylene were used, which is high for chlorine-free solvents. This result was attributed to the excellent solubility of PBDTTT-C-T in these two solvents. As previously mentioned, the intrinsic problem of spin coating is the large amount of material used and the incompatibility of this technique with continual processes occurring in a large area. Therefore, blade coating eas used for the same active layer blend of PBDTTT-C-T and [70]PCBM.

3.2. Blade coating

Fig. 5 and Table 1 shows the performance of the solar cells fabricated using blade coating in various solvents. All of the solar cells produced efficiency approximately 6% regardless of whether the solvents contained chlorine. The device constructed using toluene and xylene exhibited high efficiency of 6.09% and 6.11%, respectively. The device fabricated using chlorobenzene exhibited an efficiency

Table 1
Photovoltaic parameters for PBDTTT-C-T:[70]PCBM solar cells with active layers dissolved in different solvents by using spin-coating and blade-coating.

Cell	J_{sc} (mA/cm^2)	Voc (V)	Fill factor	PCE (%)
Toluene (spin)	13.277 ± 0.226	0.799 ± 0.002	0.535 ± 0.006	5.679 ± 0.178
Chlorobenzene (spin)	12.094 ± 0.122	0.784 ± 0.002	0.496 ± 0.004	4.712 ± 0.069
Xylene (spin)	14.471 ± 0.321	0.784 ± 0.001	0.481 ± 0.005	5.459 ± 0.064
Dichlorobenzene (spin)	13.608 ± 0.127	0.799 ± 0.001	0.586 ± 0.004	6.358 ± 0.059
Toluene (blade)	13.273 ± 0.140	0.794 ± 0.002	0.565 ± 0.016	5.954 ± 0.132
Chlorobenzene (blade)	11.793 ± 0.39	0.799 ± 0.002	0.594 ± 0.016	5.550 ± 0.207
Xylene (blade)	12.813 ± 0.260	0.809 ± 0.003	0.577 ± 0.007	5.983 ± 0.129

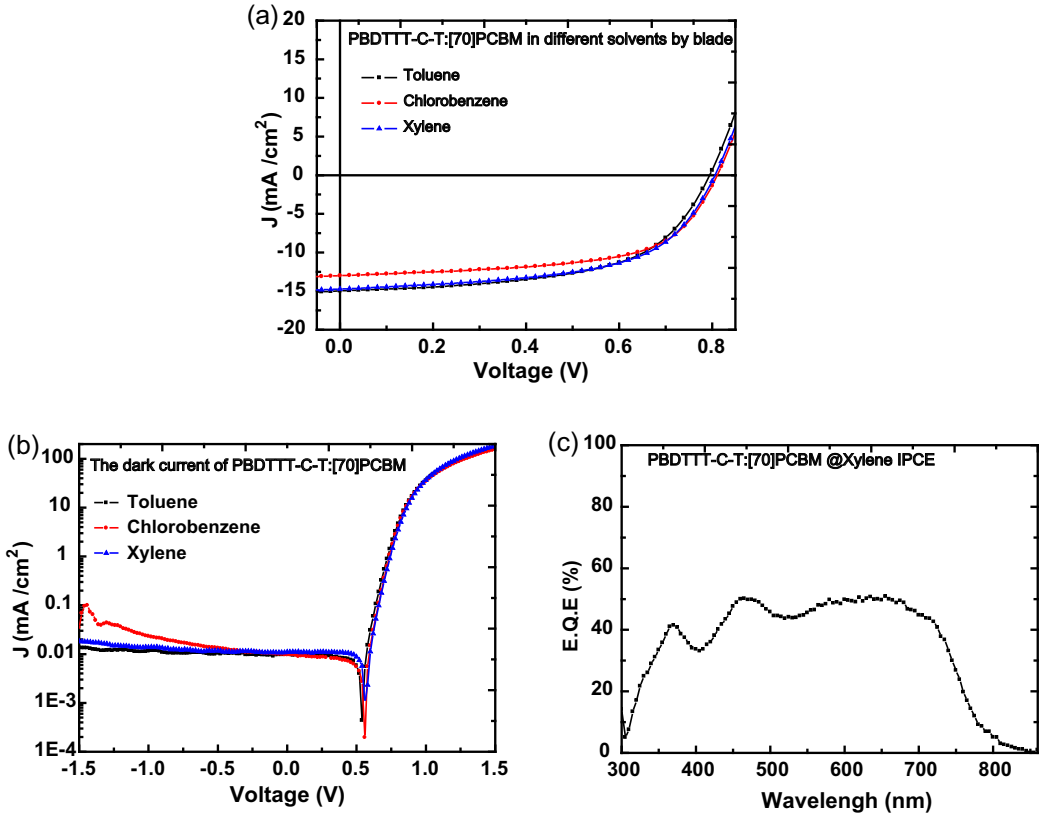

Fig. 5. (a) The *J–V* curves and (b) the dark *J–V* curves using log scale of PBDTTT-C-T/[70]PCBM solar cells with active layers dissolved in different solvents using blade coating method. (c) IPCE spectrum of PBDTTT-C-T/[70]PCBM @xylene device.

5.76%. The chlorobenzene device exhibited a lower efficiency because it produced lower short-circuit current J_{SC} than the other devices did, as shown in Fig. 5a. The dark *J–V* curves are shown in Fig. 5b using log scale. Under reverse bias, the leakage current of the devices fabricated using chlorobenzene was higher than that of the devices fabricated using by toluene and xylene. Blade coating in xylene gives the highest efficiency, and its external quantum efficiency (IPCE) for the device is shown in Fig. 5c. After multiplying the IPCE with AM1.5 solar spectrum and integration over the wavelength, the total photo-current is 12.81 mA/cm^2. This is about 10% lower than the measured J_{sc} of 14.14 mA/cm^2. In order to avoid possible overestimating the J_{sc}, we scaled it down by a factor $x = 0.906$ to match the integrated IPCE in Tables 1 and 3, which summarizes the performance. For devices conditions other than blade coating in xylene, we used the same factor x for the down scaling.

To obtain a more comprehensive insight into the origin of this moderate dependence on solvents, the absorption spectra of the pure PBDTTT-C-T film and the blend film blade coated using various solvents were measured, and the results are shown in Fig. 6. In pure PBDTTT-C-T film, the xylene film produced a pronounced long-wavelength shoulder peak at 705 nm, whereas the other two films did not produced a clear peak as shown in Fig. 6a. The cause of this shoulder peak is generally attributed to the polymer aggregates in which the ordered chain packing produces a low amount of exciton energy. Xylene exhibited the highest boiling point among the three solvents and this strong aggregate formation may have resulted from using a longer drying time under the same heating conditions used

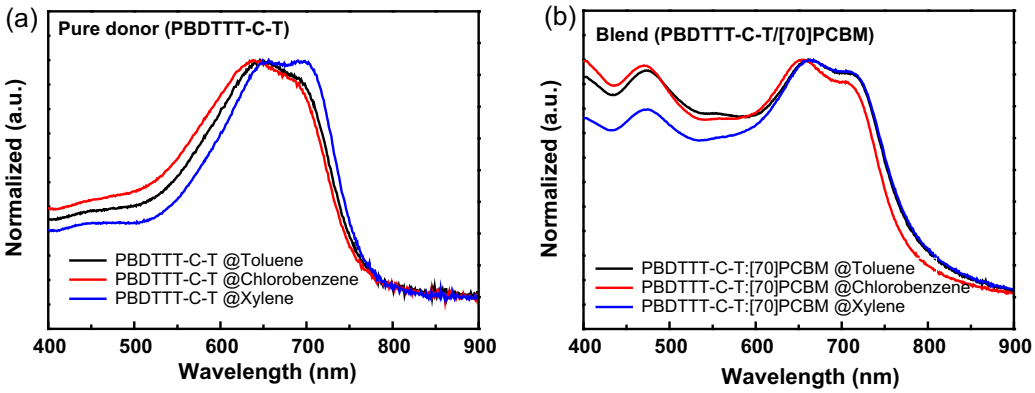

Fig. 6. The absorption spectra of films prepared with different solvents. (a) The pure PBDTTT-C-T and (b) the blend of PBDTTT-C-T/[70]PCBM.

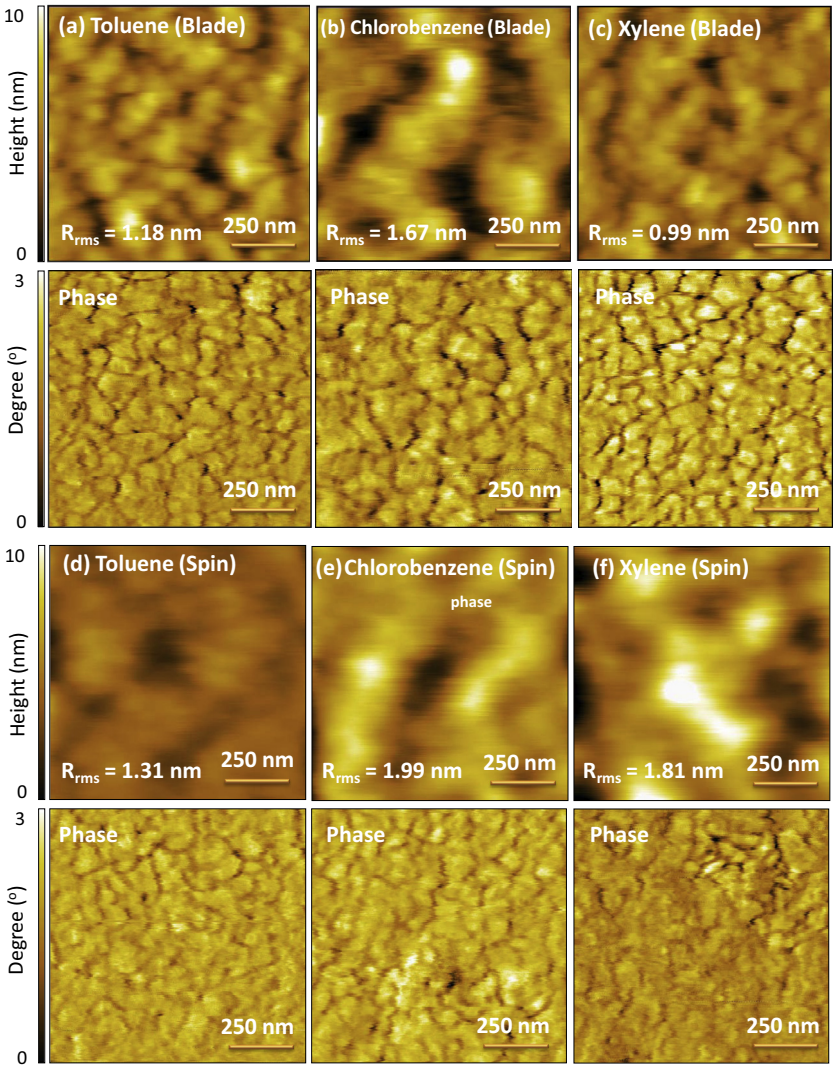

Fig. 7. AFM topography and phase images for blade (a–c) and for spin (d–f) with active layers dissolved in different solvents (1 μm × 1 μm).

in the blade coating process. However, this major difference in the absorption spectra was not visible in the blend film analysis, as shown in Fig. 6b, before and after normalization. Chlorobenzene, toluene, and xylene produced similar spectra in the 600–750 nm range and exhibited clearly visible shoulder peaks. The chlorobenzene film

exhibited a slightly lower peak than the other solvents. Therefore, this negligible difference in aggregate formation was unlikely to have caused the differences in J_{SC}, as shown in Fig. 5a.

3.3. AFM images

To understand the morphology of the films that were blade coated using various solvents further, atomic force microscope (AFM) was used to obtain the topography and phase images of the films formed using various solvents. The results are shown in Fig. 7(a–c, for blade, d–f for spin) and Table 2, with the films deposited using spin coating displayed for comparison. As shown in Fig. 7a–c, the root mean square roughness values were 1.18, 1.67, and 0.99 nm for the films composed of toluene, chlorobenzene, and xylene, respectively. The chlorobenzene film exhibited the highest roughness and the largest grain size of the films. The grains are shown at a scale of 0.3 μm, were visible only in the chlorobenzene film. To demonstrate the morphological difference further, high-resolution AFM was used to measure the chlorobenzene, toluene, and xylene films. The topography diagrams are displayed in Fig. 8. The toluene and xylene films exhibited only a small grain at the scale of 50 nm. The chlorobenzene film exhibited both a small grain of 50 nm and a large grain of 0.3 μm. This large grain structure is most likely responsible for the low J_{sc} of the chlorobenzene device, shown in Fig. 5a.

Table 2
The R_{rms} values of the PBDTTT-C-T/[70]PCBM film dissolved in various solvents by using spin-coating and blade-coating.

	Toluene (nm)	Chlorobenzene (nm)	Xylene (nm)
Blade	1.18 ± 0.19	1.67 ± 0.27	0.99 ± 0.27
Spin	1.31 ± 0.63	1.99 ± 0.65	1.81 ± 0.44

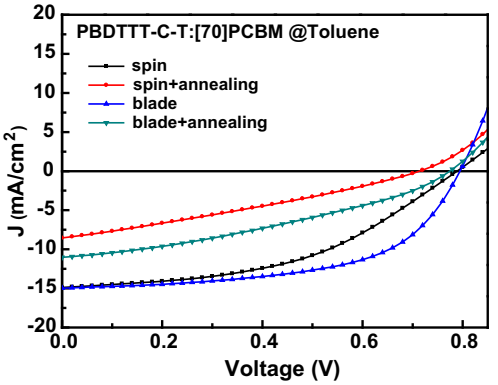

Fig. 9. *J–V* curves of PBDTTT-C-T/[70]PCBM @toluene devices, and the thermal annealing has negative effect.

This large grain structure may contain a high concentration of grain boundaries and consequently form photo-carrier recombination centers. Furthermore, the large grains may cause the film to have poor contact with the top metal cathode. High-resolution AFM exhibited higher surface roughness than the low-resolution AFM for the sample. The possible reason is that certain fine structures in the film could not be resolved by the low-resolution AFM, for example, a dip with high depth but small area. The phase image for the chlorobenzene film exhibited a high phase contrast between the center and the edge of the grain as shown in Fig. 7b. However, no high phase contrast in the toluene and xylene films was observed, as shown in Fig. 7a and c. The high phase contrast in the chlorobenzene film suggests that donor–acceptor phase separation occurred at the 0.3 μm scale, which is much higher than the exciton diffusion length of approximately 20 nm. This large-scale phase separation may reduce the total bulk hetero-junction interface concentration and lower the exciton

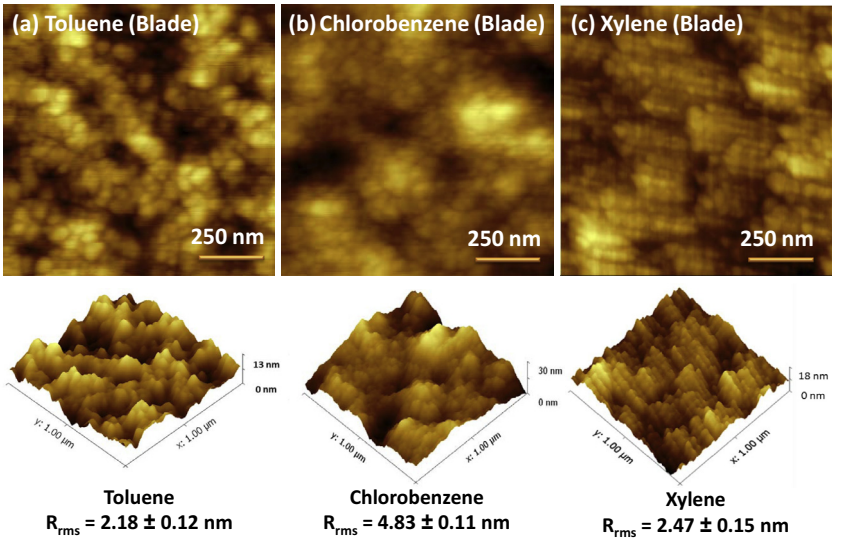

Fig. 8. The high resolution AFM topography images and R_{rms} values of the PBDTTT-C-T/[70]PCBM active layers dissolved in (a) toluene, (b) chlorobenzene and (c) xylene. The upper diagrams are 2-D images and the under diagrams are 3-D images (1 μm × 1 μm).

Table 3
Photovoltaic parameters for PBDTTT-C-T:[70]PCBM @toluene by spin-coating and blade-coating. The thermal annealing has negative effect.

Cell	J_{sc} (mA/cm^2)	Voc (V)	Fill factor	PCE (%)
Spin	13.170 ± 0.171	0.779 ± 0.010	0.446 ± 0.013	4.626 ± 0.207
Spin + annealing	7.879 ± 0.225	0.709 ± 0.008	0.311 ± 0.010	1.706 ± 0.105
Blade	13.273 ± 0.140	0.794 ± 0.002	0.565 ± 0.016	5.954 ± 0.132
Blade + annealing	10.200 ± 0.315	0.772 ± 0.002	0.353 ± 0.003	2.782 ± 0.103

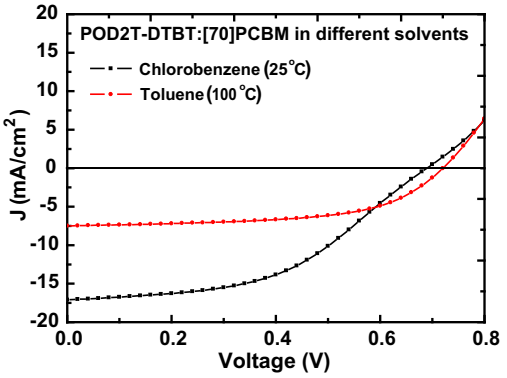

Fig. 10. *J–V* curves of POD2T-DTBT/[70]PCBM solar cells with active layers dissolved in chlorobenzene at room temperature and toluene at 100 °C.

dissociation probability. The smooth surface of the blend film with a roughness of approximately 1 nm is crucial for maintaining the stability of the device. A film with 1 nm roughness is similar to a typical spin-coated polymer film with a single component. Therefore, blade coating PBDTTT-C-T and [70] PCBM simultaneously produced an extremely smooth film and a high exciton dissociation probability. These results usually do not occur in spin coating. The AFM images for the films fabricated using spin coating are shown in Fig. 7d–f for comparison. In spin coating, the roughness of the film is generally higher than that of the films fabricated using blade coating. Large grains were visible in the chlorobenzene film. As shown in Fig. 4 the chlorobenzene also produced a lower level of efficiency than toluene and xylene did, which is similar to the trend that occurred when the devices were blade coated. The smooth surface of the blade-coated films is probably related to the rapid drying technique that was used. Simultaneously heating the films from the bottom and the top by using a hot plate and hot wind cause the films to become dry in seconds. The xylene film took 10 s to dry, whereas the toluene and chlorobenzene films took 1–3 s. Rapid drying prevented the formation of a rough structure caused by horizontal or vertical molecular migration during the drying time.

3.4. Annealing effect

In the conventional solvent annealing fabrication of polymer solar cells using dichlorobenzene, a thermal annealing step conducted after solvent annealing is performed. The efficiency increased as the microscopic morphology was tuned when using thermal annealing. Thermal annealing, however, negatively affected the PBDTTT-C-T and [70]PCBM blend film, regardless of the solvent or the deposition methods used. The effect of performing thermal annealing at 140 °C for 20 min is shown in Fig. 9 and Table 3. After completing the thermal annealing process, the efficiency decreased approximately 50% for all conditions. This suggests that the as-deposited films already possessed a nearly optimal morphology, and that further tuning using thermal annealing at a high temperature was not required.

3.5. Polymers with low solubility in toluene

Chlorinated solvents are in general stronger than the chlorine-free solvents like toluene. To illustrate the uniqueness of PBDTTT-C-T further, another two polymers dissolved in a toluene solution were studied. The first polymer was POD2T-DTBT, which had a low band-gap of 1.6 eV and exhibited a high efficiency of 6.26% when conventional annealing was used [27] and 6.67% when blade coating and chlorobenzene were used [25,28]. The other polymer was the archetypical polymer P3HT, which exhibited an efficiency of approximately 4% when solvent annealing was used. Unlike PBDTTT-C-T, both POD2T-DTBT and P3HT exhibited poor solubility in chlorine-free solvents. For example, the blend with a concentration of 19 mg/ml and a 1:1 P3HT:[60]PCBM ratio were fully dissolved in dichlorobenzene overnight, but they required two days to dissolve in toluene. The solubility of POD2T-DTBT in toluene was extremely low, which indicates that performing blade coating with this solution at room temperature is impossible. A uniform film could be fabricated only by heating the toluene solution to 100 °C. The solar cell characteristics of POD2T-DTBT blended with [70]PCBM by heating a toluene solution are shown in Fig. 10 and Table 4. In contrast to PBDTTT-C-T, the toluene device exhibited a significantly low efficiency of 3.16% compared with the 5.62% exhibited

Table 4
Photovoltaic parameters for POD2T-DTBT/[70]PCBM solar cells with active layers dissolved in different solvents by blade-coating.

Cell	J_{sc} (mA/cm^2)	Voc (V)	Fill factor	PCE (%)
Chlorobenzene (25 °C)	16.610 ± 0.302	0.690 ± 0.001	0.485 ± 0.015	5.573 ± 0.045
Toluene (100 °C)	7.666 ± 0.241	0.723 ± 0.002	0.565 ± 0.013	3.128 ± 0.034

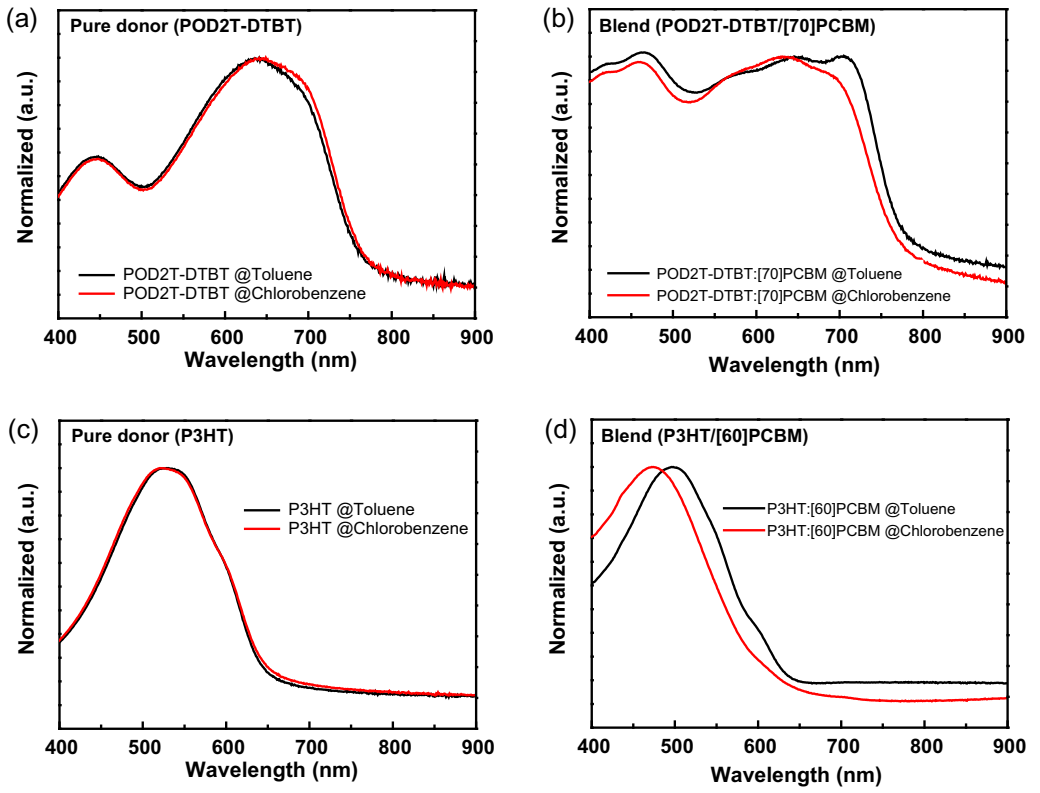

Fig. 11. The absorption spectra of films prepared with different solvents. (a) The pure POD2T-DTBT, (b) POD2T-DTBT/[70]PCBM, (c) the pure P3HT and (d) P3HT/[60]PCBM.

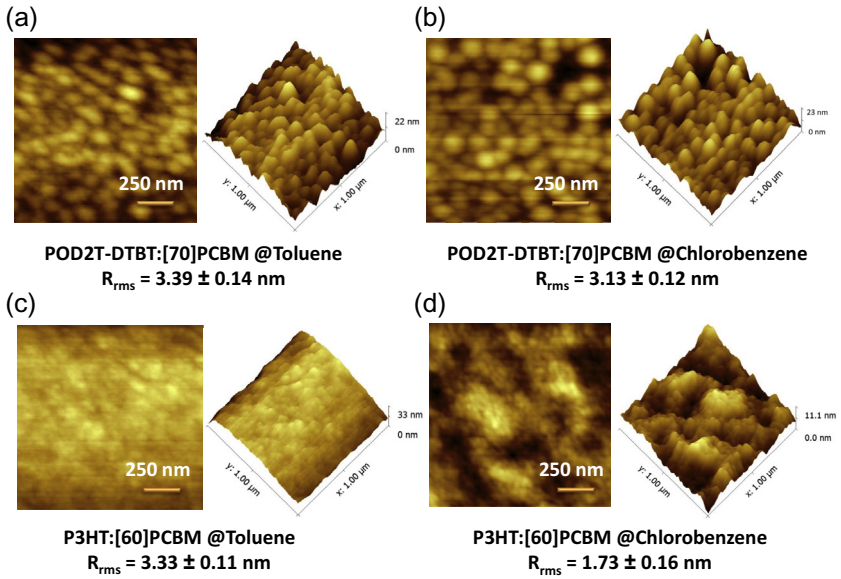

Fig. 12. AFM topography images and R_{rms} values of the POD2T-DTBT/[70]PCBM and P3HT/[60]PBCM active layers dissolved in (ac) toluene and (bd) chlorobenzene (1 μm × 1 μm for 2-D and 3-D images).

by the chlorobenzene device. Therefore, to obtain high efficiency when using a chlorine-free solvent, applying a molecular design for achieving high solubility is necessary.

The absorption spectra of the pure POD2T-DTBT film and the blend film are shown in Fig. 11a, and b. The spectra of the pure toluene and chlorobenzene films were almost

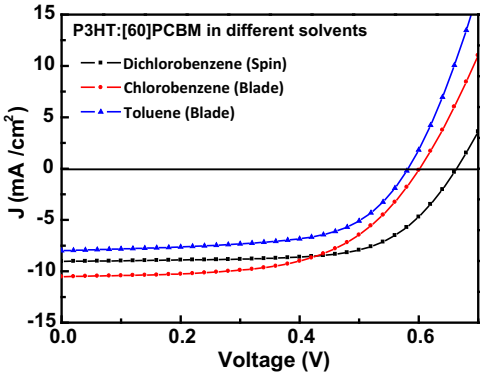

Fig. 13. *J–V* curves of P3HT/[60]PCBM solar cells with active layers dissolved in various solvents.

identical. The blend film spectra displayed a distinct absorption shoulder of approximately 705 nm when POD2T-DTBT was dissolved in toluene, but this did not occur in the spectra produced when chlorobenzene was used. This implies that the high concentration of POD2T-DTBT aggregate was caused by the poor solubility of the polymer in toluene. Similarly, the pure P3HT film produced an almost identical absorption spectra when toluene and chlorobenzene were used, as shown in Fig. 11c. By contrast, the blend film spectra displayed a clear red shift when POD2T-DTBT and [70]PCBM were dissolved in toluene, which may have been caused by the P3HT aggregate that formed because of poor solubility. In contrast to POD2T-DTBT and P3HT, the absorption spectrum of the PBDTTT-C-T blend film exhibited little solvent dependence, as shown in Fig. 6. This characteristic is associated with the excellent solubility of PBDTTT-C-T in chlorine-free solvents. The high-resolution AFM images for the POD2T-DTBT and P3HT blend film when toluene and chlorobenzene were used are shown in Fig. 12 for toluene and chlorobenzene. Distinct granular structures were observed in the chlorobenzene films, but not in the toluene films. This grain structure suggests that proper donor–acceptor phase separation is required to achieve a high exciton dissociation rate. As shown in Figs. 10 and 13, and Tables 4 and 5, the toluene device exhibited much lower efficiency than did the chlorobenzene devices for the two polymers. Therefore, the poor efficiency produced when using toluene is related to the lack of phase separation at the proper length scale. By contrast, the granular structures of the PBDTTT-C-T film were noticeable even when the polymer was dissolved in toluene, as shown in Fig. 8a. Therefore, the key criteria for achieving high performance using a chlorine-free solvent is the high solubility of the polymer and the formation of granular structures at the 20–50 nm length scale.

Finally, we remarked on the need for heating of the blend solution used in coating. Full dissolution of the PBDTTT-C-T is possible only with heating to 80 °C for all solvents in this work. The solution became a gel once the temperature drops back to room temperature. The coating

Table 5
Photovoltaic parameters for P3HT/[60]PCBM solar cells with active layers dissolved in different solvents by blade-coating.

Cell	J_{sc} (mA/cm^2)	Voc (V)	Fill factor	PCE (%)
Dichlorobenzene (spin)	8.919 ± 0.106	0.661 ± 0.003	0.654 ± 0.008	3.856 ± 0.107
Chlorobenzene (blade)	10.317 ± 0.209	0.602 ± 0.001	0.581 ± 0.005	3.607 ± 0.040
Toluene (blade)	7.855 ± 0.145	0.589 ± 0.001	0.605 ± 0.005	2.783 ± 0.047

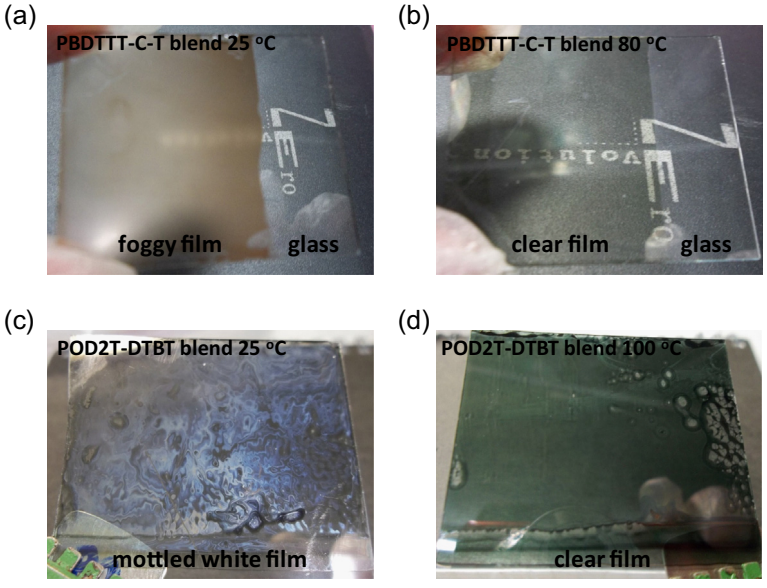

Fig. 14. PBDTTT-C-T and POD2T-DTBT blends were blade coated at different temperature.

of the gel gave a foggy film with high roughness as shown in Fig. 14a. Therefore, all the devices are coated with heated solution to ensure a clear film with low roughness as shown in Fig. 14b. As for the POD2T-DTBT, it was fully dissolved in toluene only with heating up to 100 °C. Once the solution was cooled down to room temperature, instead of gelation there are precipitates. Coating of solution at room temperature also gives foggy rough film similar to PBDTTT-C-T films. The film was mottled white as shown in Fig. 14c. Coating of toluene solution at 100 °C gives clear film as shown in Fig. 14d. POD2T-DTBT can be fully dissolved in chlorobenzene and coated at room temperature.

4. Conclusion

In summation, a high-performance polymer solar cell based on PBDTTT-C-T was successfully fabricated using blade coating in toluene and xylene solution. These solvents are chlorine-free. Therefore, the conventional use of toxic solvents such as dichlorobenzene and chlorobenzene in polymer solar cells can be avoided. The highest efficiency achievable by spin coating was 6.42%, and that for blade coating was 6.11%. The good solubility of PBDTTT-C-T in the chlorine-free solvents was the primary reason for the high performance. By combining a non-toxic solvent with blade coating, which is suitable for roll-to-roll fabrication with minimal material waste, efficient polymer solar cells can be fabricated in high volumes, using an environmentally-friendly approach.

Acknowledgements

This work was supported by the National Science Council of Taiwan under Grant Nos. 103-2120-M-009-003-CC1, 102-2221-E-007-125-MY3, 101-2112-M-009-006-MY3, 101-2112-M-007-017-MY3 and the Ministry of Economic Affairs of Taiwan under Grant No. 100-EC-17-A-07-S1-157. We thank Wen-Bin Jian for the high-resolution AFM images.

Reference

[1] Z. He, C. Zhong, S. Su, M. Xu, H. Wu, Y. Cao, Nat. Photonics 6 (2012) 591–595.
[2] Y.-W. Su, S.-C. Lan, K.-H. Wei, Mater. Today 15 (2012) 554–562.
[3] L. Ye, S. Zhang, W. Ma, B. Fan, X. Guo, Y. Huang, H. Ade, J. Hou, Mater. Views 24 (2012) 6335–6341.
[4] X. Guo, M. Zhang, J. Tan, S. Zhang, L. Huo, W. Hu, Y. Li, J. Hou, Adv. Mater. 24 (2012) 6536–6541.
[5] Y. Liang, Z. Xu, J. Xia, S.-T. Tsai, Y. Wu, G. Li, C. Ray, L. Yu, Adv. Mater. 22 (2012) E135–E138.
[6] H.Y. Chen, J.H. Hou, S.Q. Zhang, Y.Y. Liang, G.W. Yang, Y. Yang, L.P. Yu, Y. Wu, G. Li, Nat. Photonics 3 (2009) 649–653.
[7] S.C. Price, A.C. Stuart, L. Yang, H. Zhou, W. You, J. Am. Chem. Soc. 133 (2011) 4625–4631.
[8] C. Piliego, T.W. Holcombe, J.D. Douglas, C.H. Woo, P.M. Beaujuge, J.M.J. Fréchet, J. Am. Chem. Soc. 132 (2010) 7595–7597.
[9] Z. He, C. Zhong, X. Huang, W.Y. Wong, H. Wu, L. Chen, S. Su, Y. Cao, Adv. Mater. 23 (2011) 4636–4643.
[10] G. Li, V. Shrotriya, J. Huang, Y. Yao, T. Moriarty, K. Emery, Y. Yang, Nat. Mater. 4 (2005) 864–868.
[11] P.A. Troshin, D.K. Susarova, E.A. Khakina, A.A. Goryachev, O.V. Borshchev, S.A. Ponomarenko, V.F. Razumova, N.S. Sariciftci, J. Mater. Chem. 22 (2012) 18433–18441.
[12] P.A. Troshin, H. Hoppe, J. Renz, M. Egginger, J.Y. Mayorova, A.E. Goryachev, A.S. Peregudov, R.N. Lyubovskaya, G. Gobsch, N.S. Sariciftci, V.F. Razumov, Adv. Funct. Mater. 19 (2009) 779–788.
[13] C.-K. Lee, C.-W. Pao, J. Phys. Chem. C 116 (2012) 12455–12461.
[14] H. Hoppe, T. Glatzel, M. Niggemann, W. Schwinger, F. Schaeffler, A. Hinsch, M.C. Lux-Steiner, N. Sariciftci, Thin Solid Films 511–512 (2006) 587–592.
[15] H. Hoppe, N.S. Sariciftci, J. Mater. Chem. 16 (2006) 45–61.
[16] S.E. Shaheen, C. Brabec, N.S. Saricifci, F. Padinger, T. Fromherz, J.C. Hummelen, Appl. Phys. Lett. 78 (2001) 841–843.
[17] M.T. Rispens, A. Meetsma, R. Rittberger, C.J. Brabec, N.S. Sariciftci, J.C. Hummelen, Chem. Commun. (2003) 2116–2118.
[18] C.M. Björström, K.O. Magnusson, E. Moons, Synth. Met. 152 (2005) 109–112.
[19] F. Reisdorffer, O. Haas, P. Le Rendu, T.P. Nguyen, Synth. Met. 161 (2012) 2544–2548.
[20] S.K. Jang, S.C. Gong, H.J. Chang, Synth. Met. 162 (2012) 426–430.
[21] K.-S. Chen, H.-L. Yip, C.W. Schlenker, D.S. Ginger, A.K.-Y. Jen, Org. Electron. 13 (2012) 2870–2878.
[22] L. Huo, S. Zhang, X. Guo, F. Xu, Y. Li, J. Hou, Angew. Chem. Int. Ed. 50 (2011) 9697–9702.
[23] S.-R. Tseng, H.-F. Meng, K.-C. Lee, S.-F. Horng, Appl. Phys. Lett. 93 (2008) 153308.
[24] C.-Y. Chen, H.-W. Chang, Y.-F. Chang, B.-J. Chang, Y.-S. Lin, P.-S. Jian, H.-C. Yeh, H.-T. Chien, E.-C. Chen, Y.-C. Chao, H.-F. Meng, H.-W. Zan, H.-W. Lin, S.-F. Horng, Y.-J. Cheng, F.-W. Yen, I.-F. Lin, H.-Y. Yang, K.-J. Huang, M.-R. Tseng, J. Appl. Phys. 110 (2011) 094501.
[25] S.-L. Lim, E.-C. Chen, C.-Y. Chen, K.-H. Ong, Z.-K. Chen, H.-F. Meng, Sol. Energy Mater. Sol. Cells 107 (2012) 292–297.
[26] Y.-F. Chang, Y.-C. Chiu, H.-C. Yeh, H.-W. Chang, C.-Y. Chen, H.-F. Meng, H.-W. Lin, H.-L. Huang, T.-C. Chao, M.-R. Tseng, H.-W. Zan, S.-F. Horng, Org. Electron. 13 (2012) 2149–2155.
[27] K.-H. Ong, S.-L. Lim, H.-S. Tan, H.-K. Wong, J. Li, Z. Ma, L.C.H. Moh, S.-H. Lim, J.C. de Mello, Z.-K. Chen, Adv. Mater. 23 (2011) 1409–1413.
[28] R. Kroon, M. Lenes, J.C. Hummelen, P.W.M. Blom, B. De Boer, Polym. Rev. 48 (2008) 531–582.